Supporting Information

Anthryl-Functionalized Cyanide-Bridged Fe/Co Cubes

Qi Liu, Yue Cheng, Shihao Liu, Zi-Yi Chen,* and Yuan-Zhu Zhang*

Contents

Figure S1. Powder X-ray diffraction (PXRD) pattern of **1**.

Figure S2. Powder X-ray diffraction (PXRD) pattern of **2**.

Figure S3. Thermal Gravimetric Analysis of **1**.

Figure S4. Thermal Gravimetric Analysis of **2**.

Figure S5. Solid-state IR spectra at room temperature of **1** and **2**.

Figure S6. Variable-temperature magnetic susceptibilities of complex **1**.

Figure S7. Variable-temperature magnetic susceptibilities of complex **2**.

Figure S8. Solid-state UV-vis spectra of **1**.

Figure S9. Solid-state UV-vis spectra of **2**.

Figure S10. UV-vis spectra of **1** in MeCN.

Figure S11 UV-vis spectra of ligand TpEtOAn in MeCN.

Figure S12. Solid-state emission (λ_{ex} = 350 nm) and excitation (λ_{em} = 420 nm) spectra of complex **1**.

Figure S13. Emission (λ_{ex} = 350 nm) spectra of complex **1** at solid state and in MeCN.

Figure S14. Solid-state emission (λ_{ex} = 360 nm) and excitation (λ_{em} = 444 nm) spectra of ligand TpEtOAn.

Figure S15. Emission (λ_{ex} = 350 nm) and excitation (λ_{em} = 420 nm) spectra of complex **2** in MeCN.

Figure S16. Excitation (λ_{em} = 420 nm) spectra of the mixture of **1** and PFN in MeCN.

Figure S17. Emission (λ_{ex} = 310 nm) and excitation (λ_{em} = 355 nm) spectra of PFN in MeCN.

Scheme S1. Synthesis route of ligand TpEtOAn.

Figure S18. ^{1}H NMR (400 MHz) spectra of TpEtOAn in $CDCl_3$.

Figure S19. ^{13}C NMR (101 MHz) spectra of TpEtOAn in CD_3CN.

Figure S20. Anthracene dimmer in crystal of **1** and **2**.

Table S1. Single Crystal diffraction data of **1** and **2**.

Table S2. The selected bond length of complex **1**.

Table S3. Selected bond length of complex **2**.

Table S4. Average Co–N bond length and continuous shape measurement of Co centers.

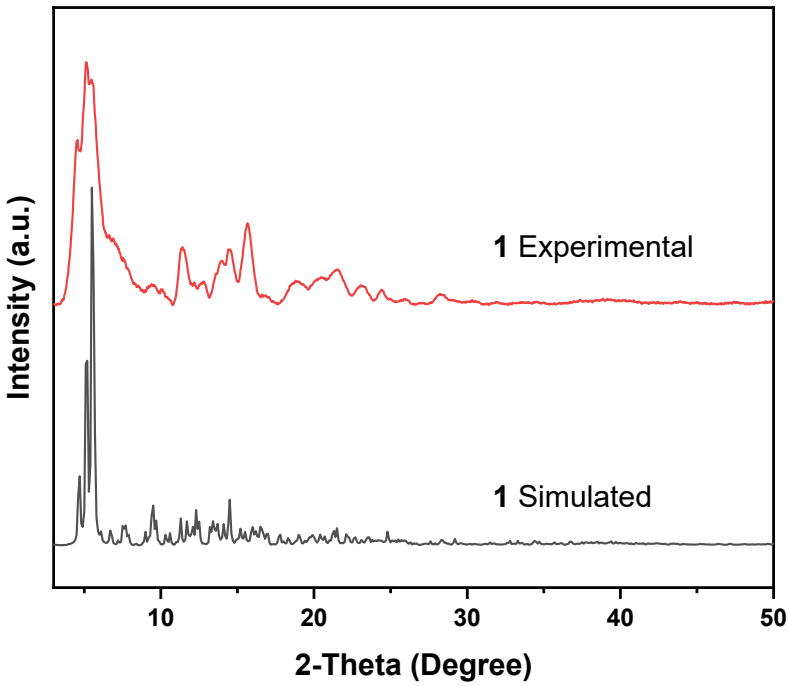

Figure S1. Powder X-ray diffraction (PXRD) pattern of **1**.

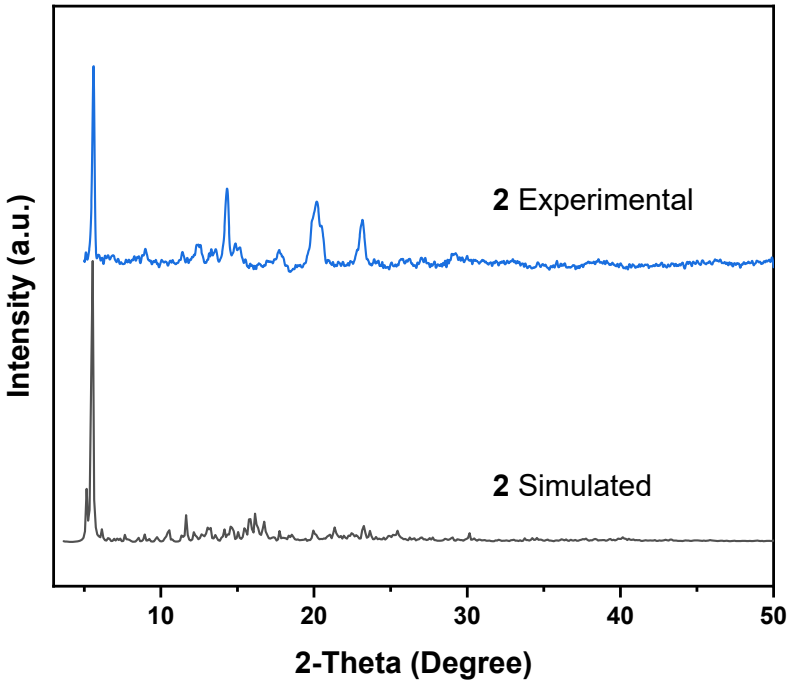

Figure S2. Powder X-ray diffraction (PXRD) pattern of **2**.

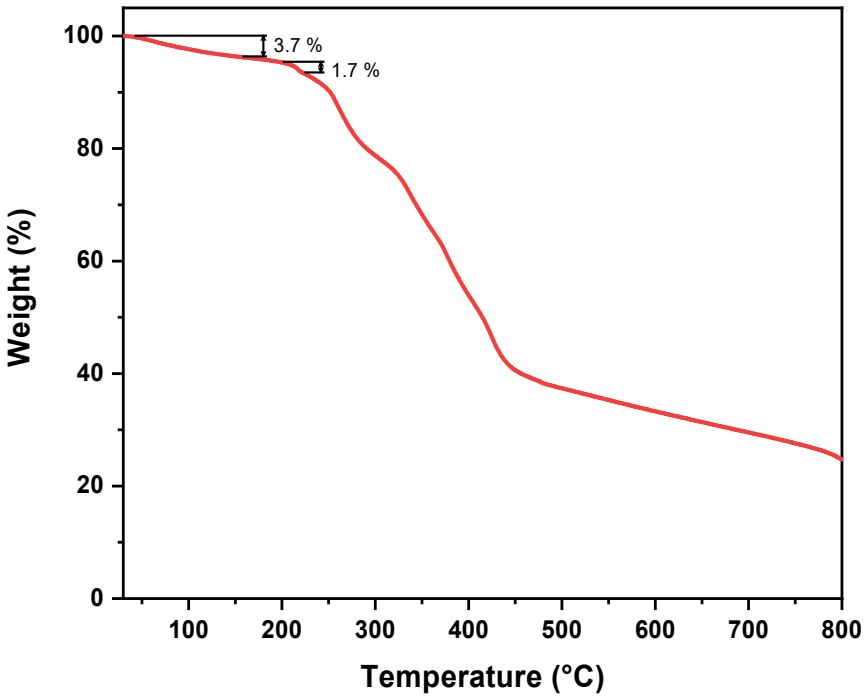

Figure S3. Thermal Gravimetric Analysis of **1**.

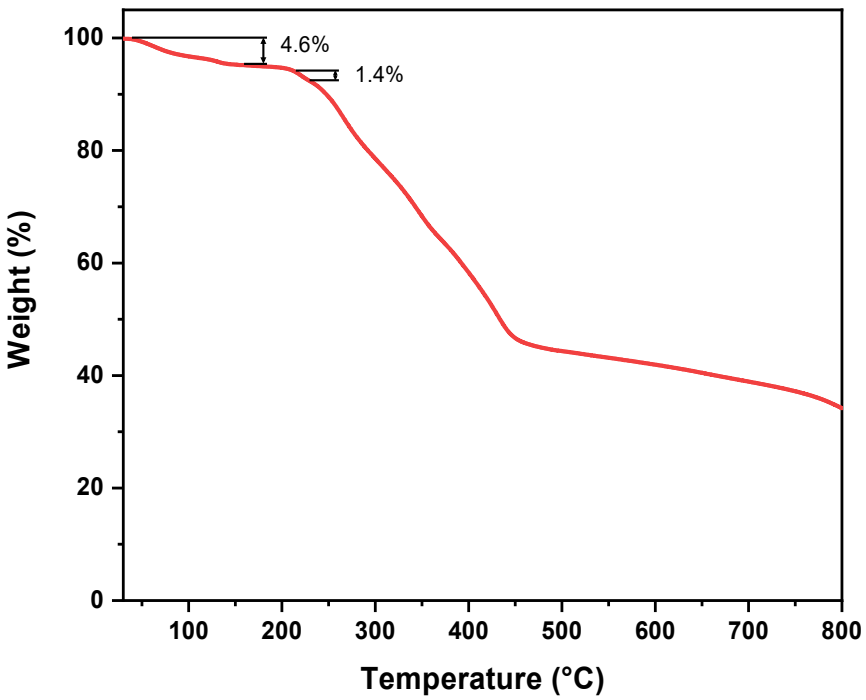

Figure S4. Thermal Gravimetric Analysis of **2**.

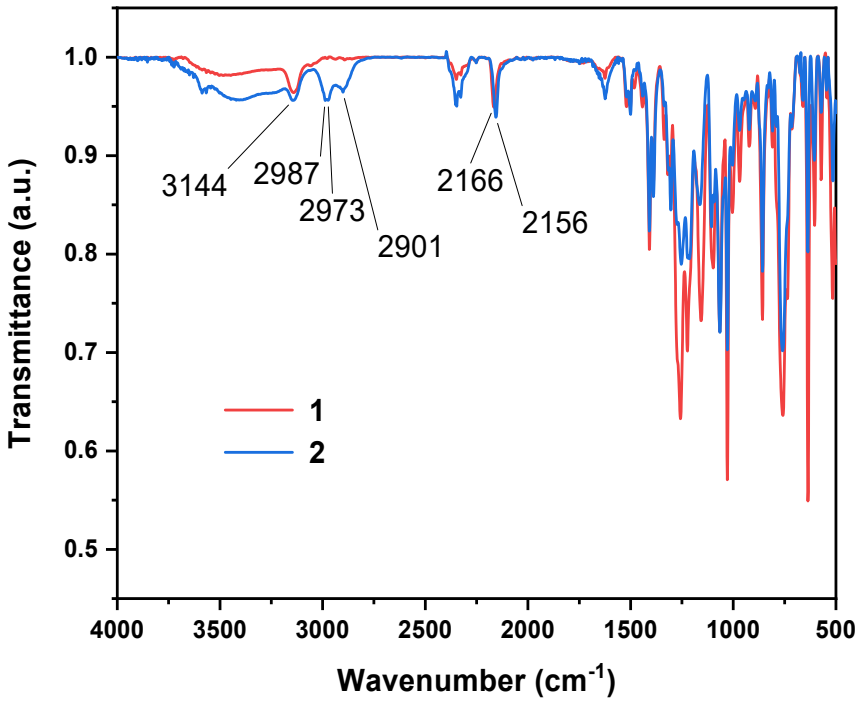

Figure S5. Solid-state IR spectra at room temperature of **1** and **2**.

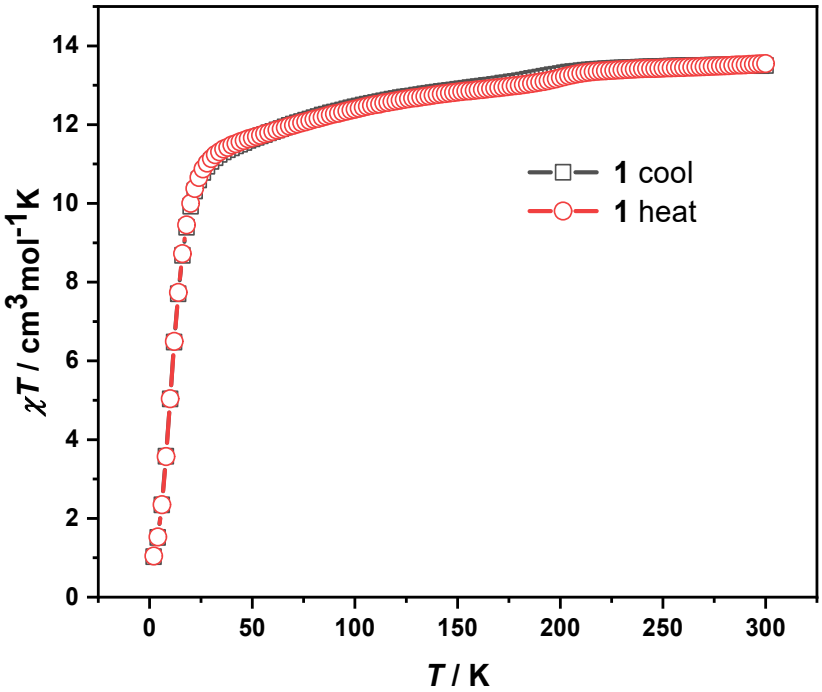

Figure S6. Variable-temperature magnetic susceptibilities of complex **1**.

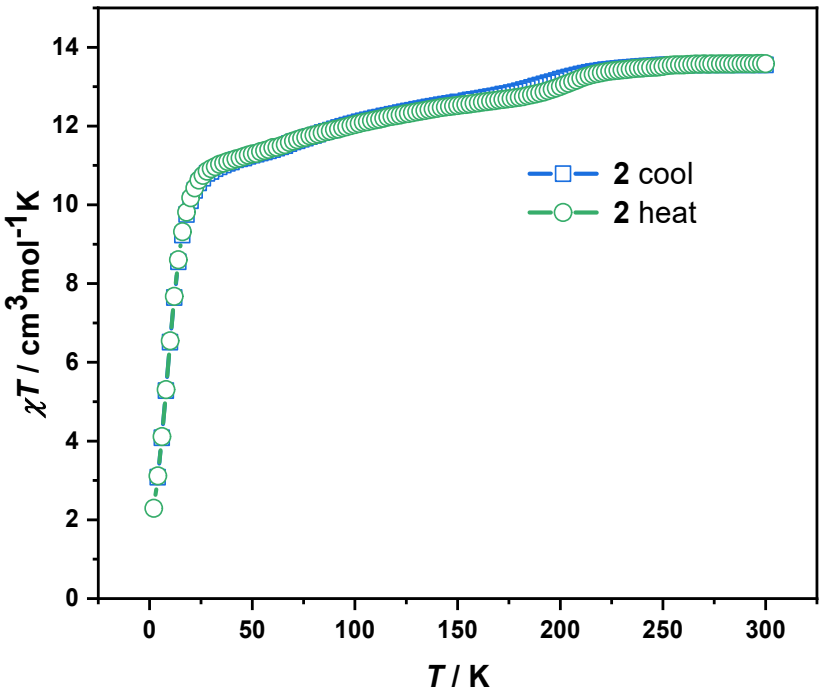

Figure S7. Variable-temperature magnetic susceptibilities of complex **2**.

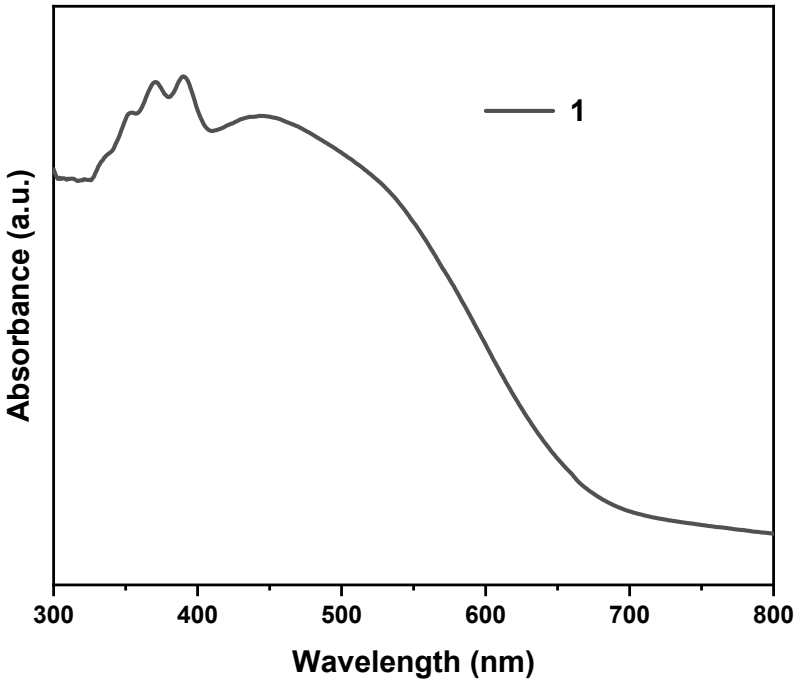

Figure S8. Solid-state UV-vis spectra of **1**.

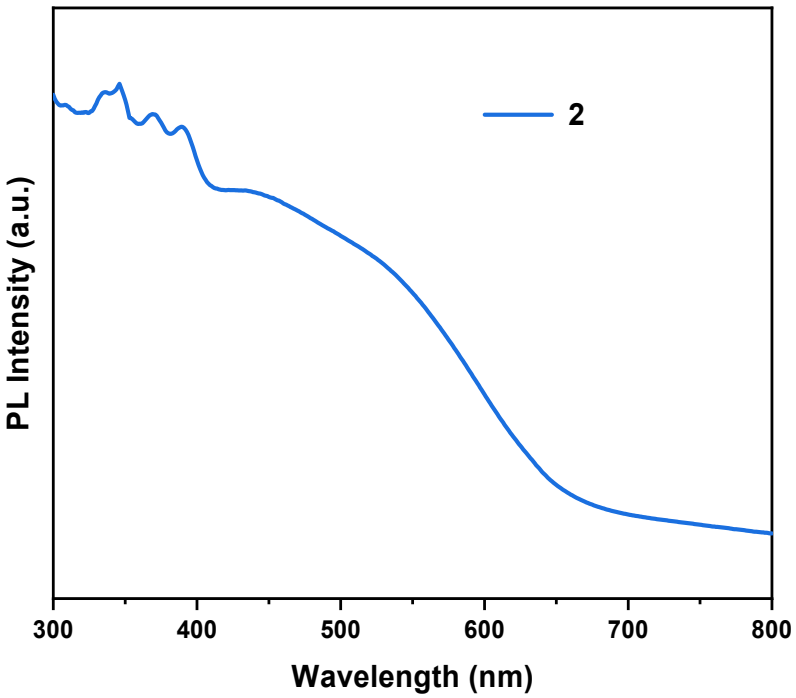

Figure S9. Solid-state UV-vis spectra of **2**.

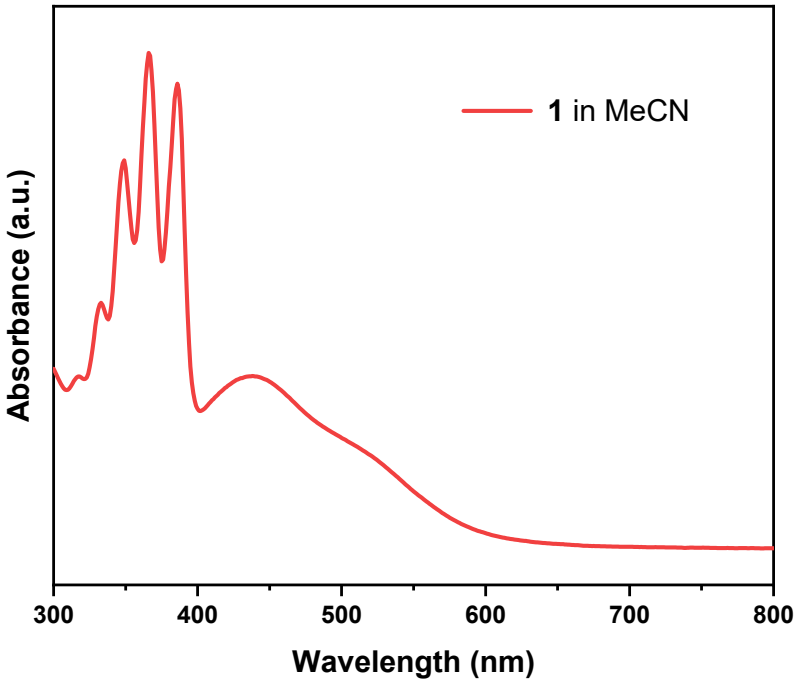

Figure S10. UV-vis spectra of **1** in MeCN.

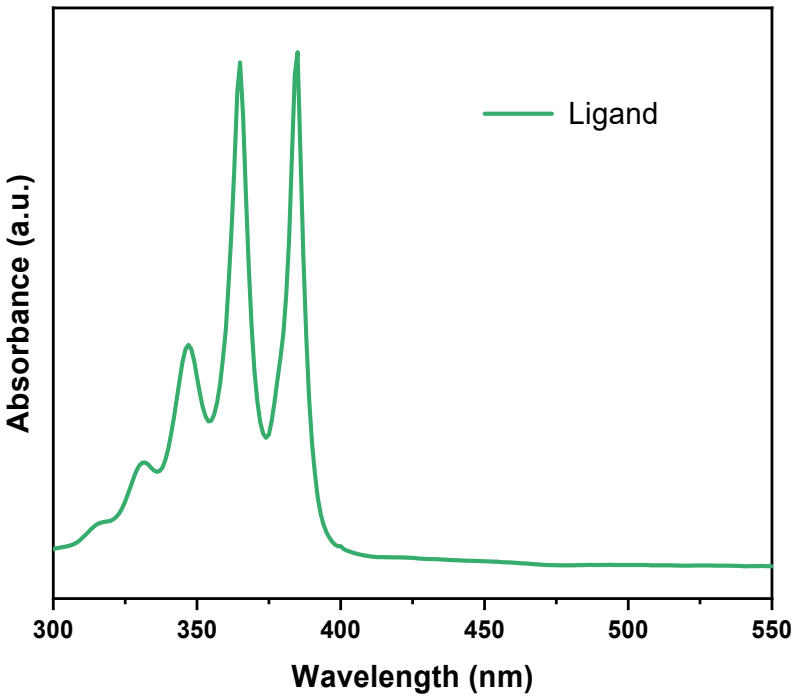

Figure S11. UV-vis spectra of ligand TpEtOAn in MeCN.

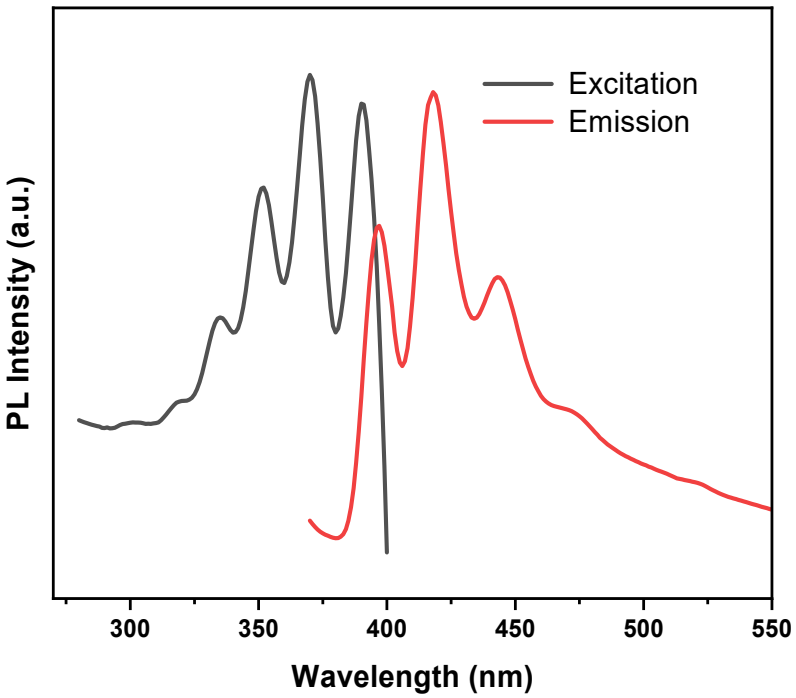

Figure S12. Solid-state emission (λ_{ex} = 350 nm) and excitation (λ_{em} = 420 nm) spectra of complex **1**.

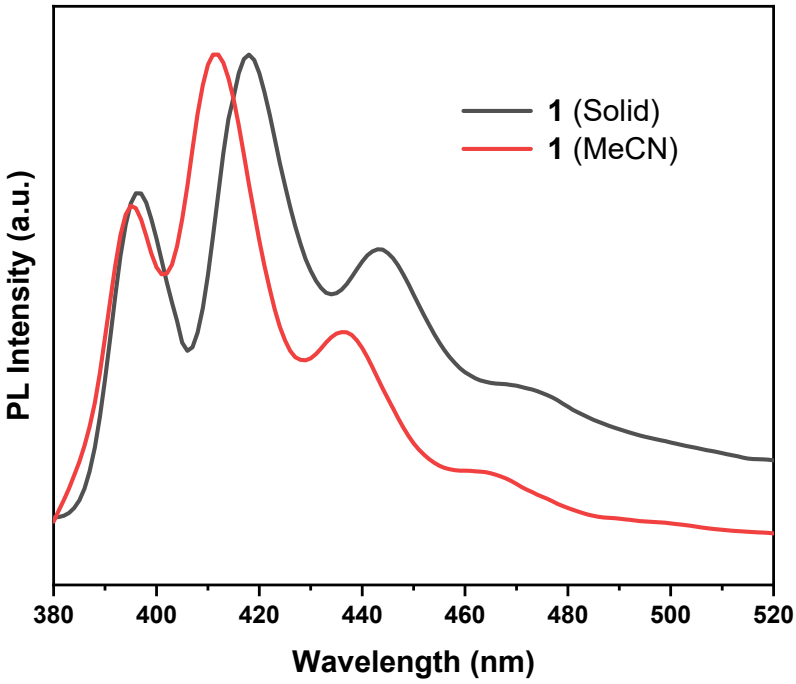

Figure S13. Emission (λ_{ex} = 350 nm) spectra of complex **1** at solid state and in MeCN.

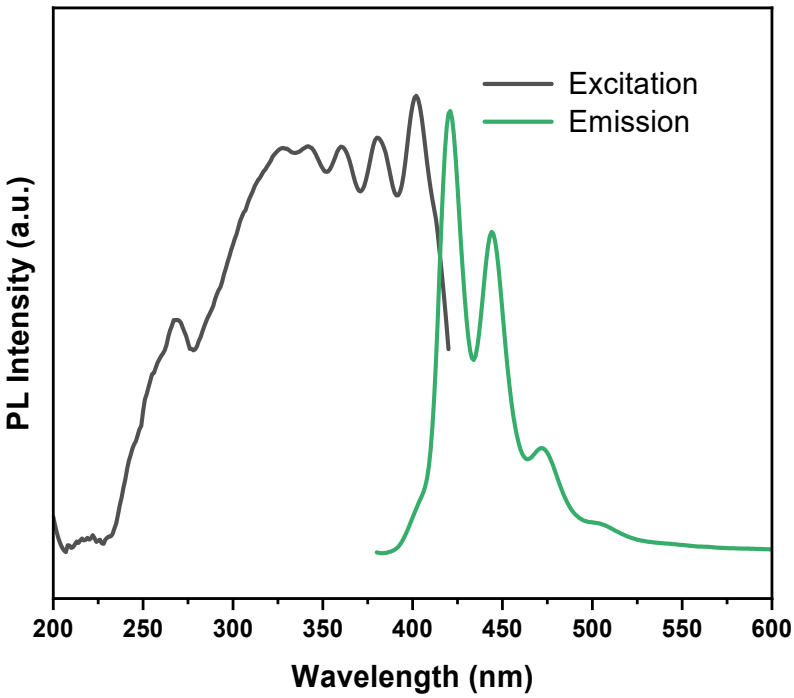

Figure S14. Solid-state emission (λ_{ex} = 360 nm) and excitation (λ_{em} = 444 nm) spectra of ligand TpEtOAn.

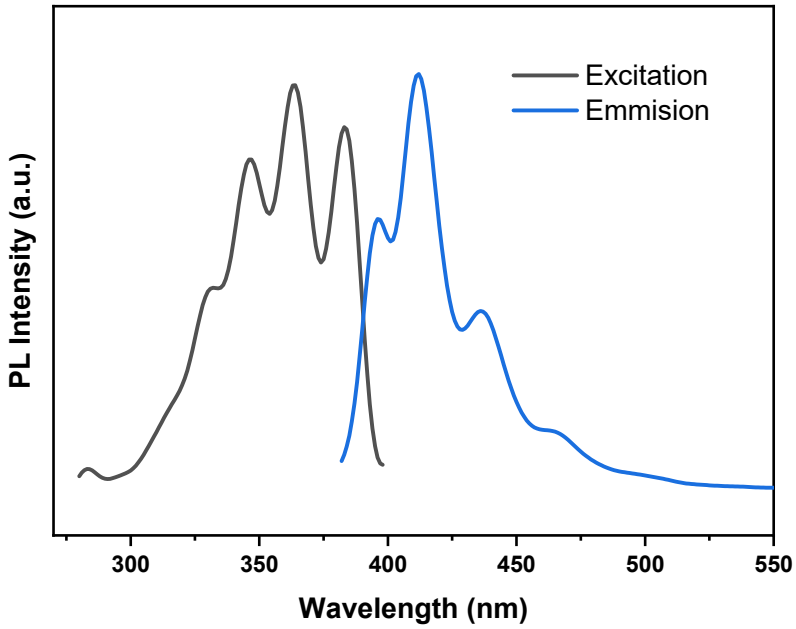

Figure S15. Emission (λ_{ex} = 350 nm) and excitation (λ_{em} = 420 nm) spectra of complex **2** in MeCN.

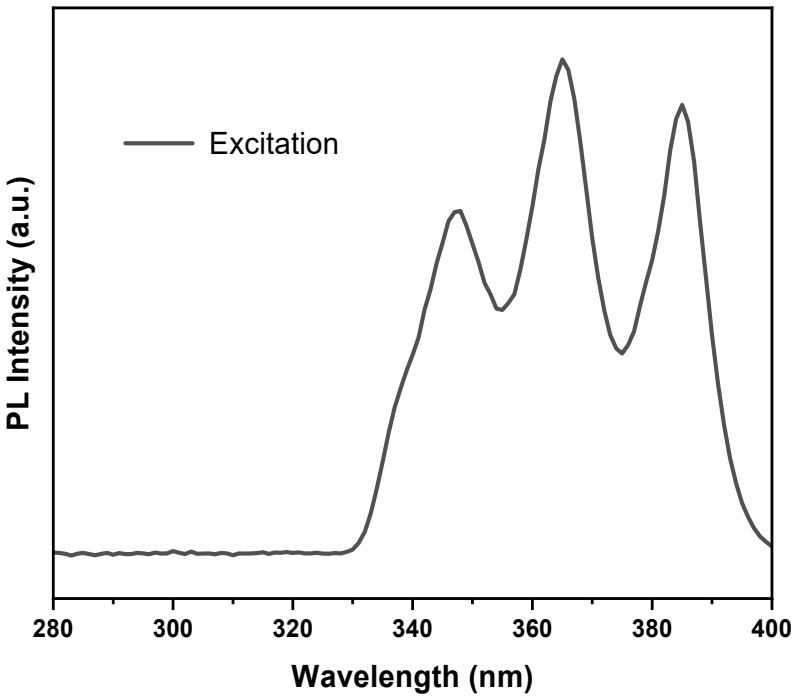

Figure S16. Excitation (λ_{em} = 420 nm) spectra of the mixture of **1** and PFN in MeCN.

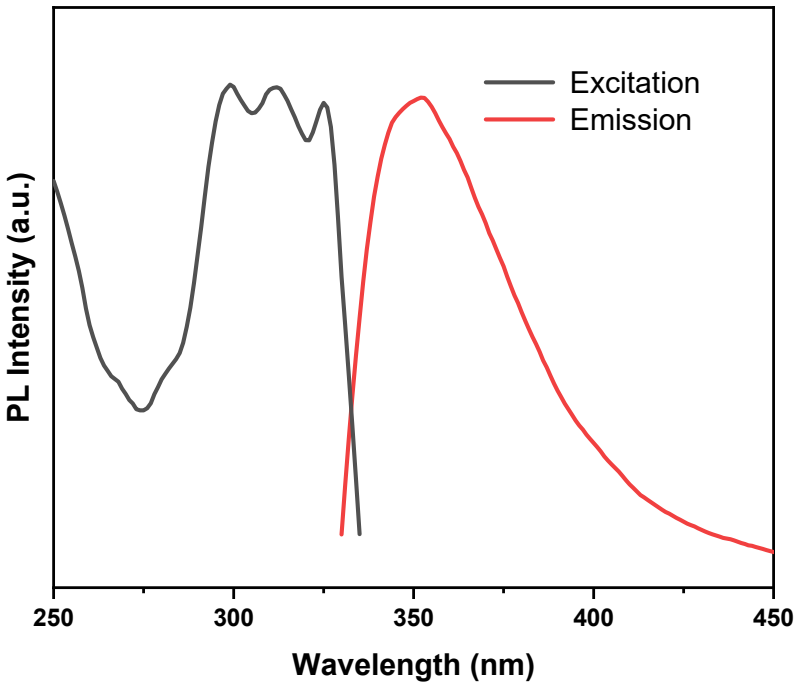

Figure S17. Emission (λ_{ex} = 310 nm) and excitation (λ_{em} = 355 nm) spectra of PFN in MeCN.

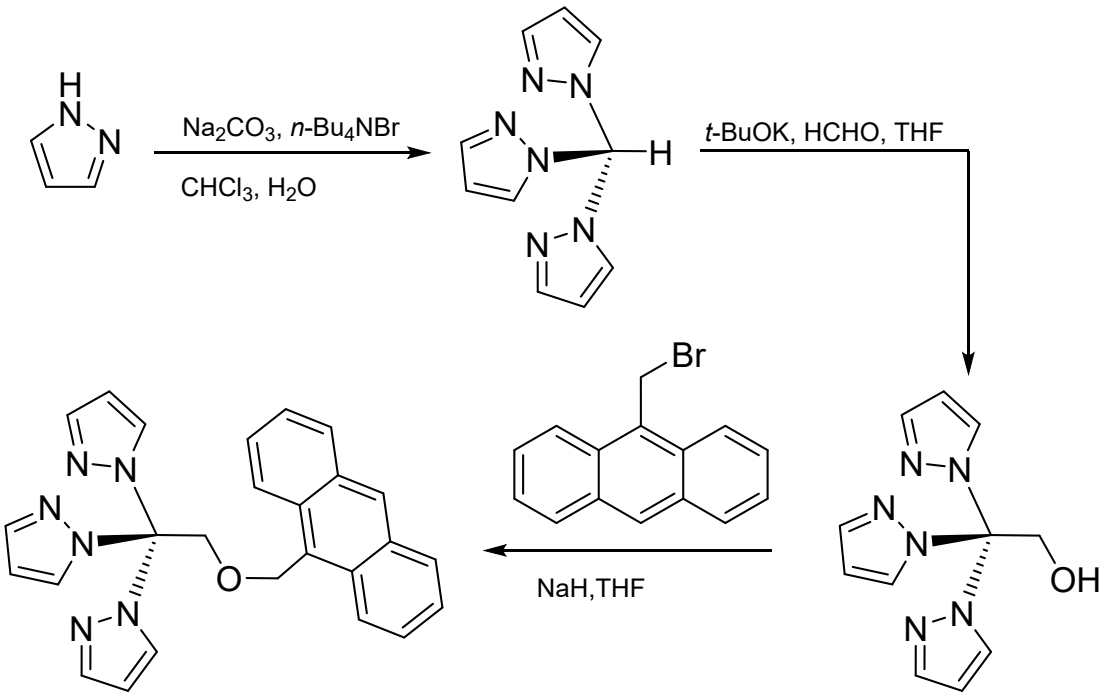

Scheme S1. Synthesis route of ligand TpEtOAn.

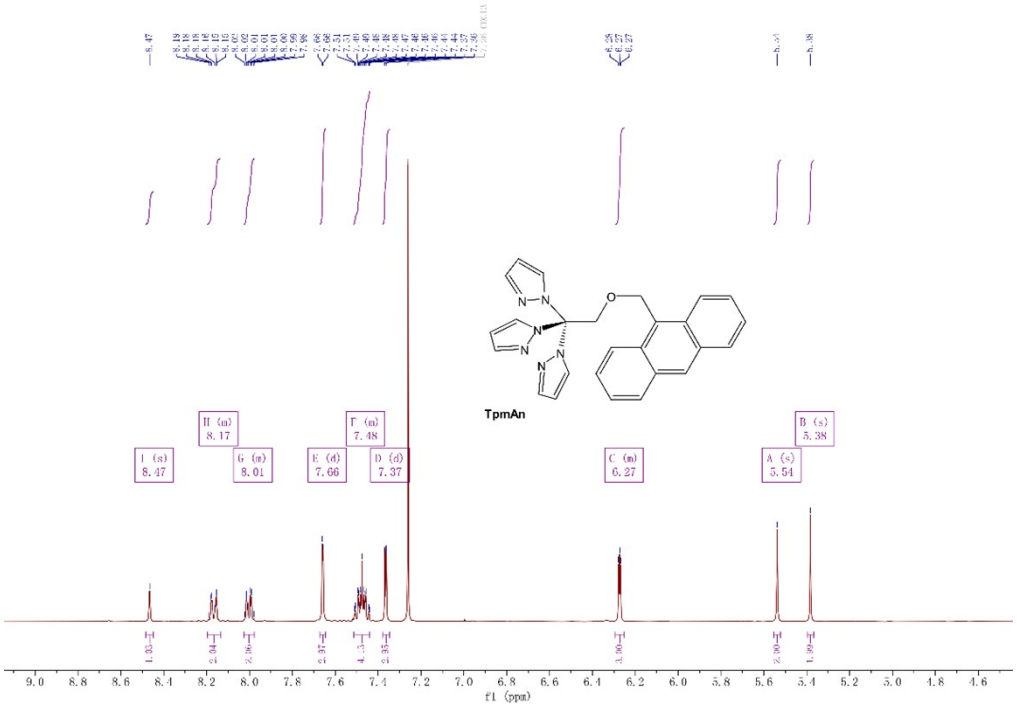

Figure S18. ^{1}H NMR (400 MHz) spectra of TpEtOAn in $CDCl_3$.

^{1}H NMR (400 MHz, $CDCl_3$) δ 8.47 (s, 1H), 8.20 – 8.14 (m, 2H), 8.03 – 7.98 (m, 2H), 7.66 (d, *J* = 1.8 Hz, 3H), 7.51 – 7.44 (m, 4H), 7.37 (d, *J* = 3.4 Hz, 3H), 6.29 – 6.25 (m, 3H), 5.54 (s, 2H), 5.38 (s, 2H).

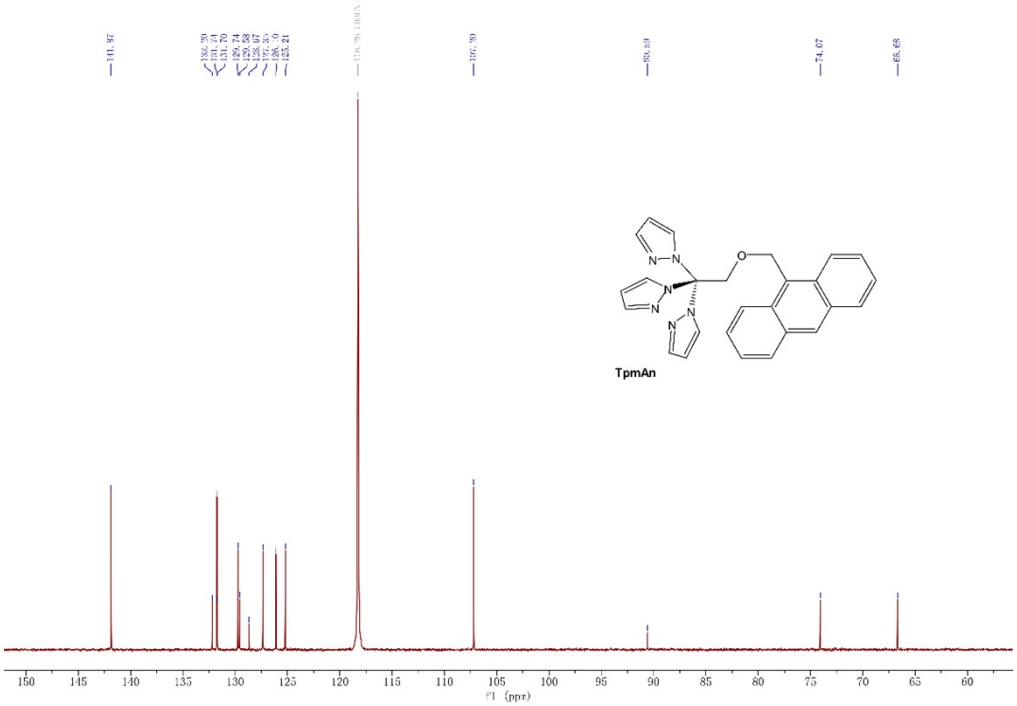

Figure S19. ^{13}C NMR (101 MHz) spectra of TpEtOAn in CD_3CN.

^{13}C NMR (101 MHz, CD_3CN) δ 141.51, 131.84, 131.38, 129.38, 129.22, 128.31, 126.99, 125.74, 124.85, 106.84, 90.23, 73.71, 66.32.

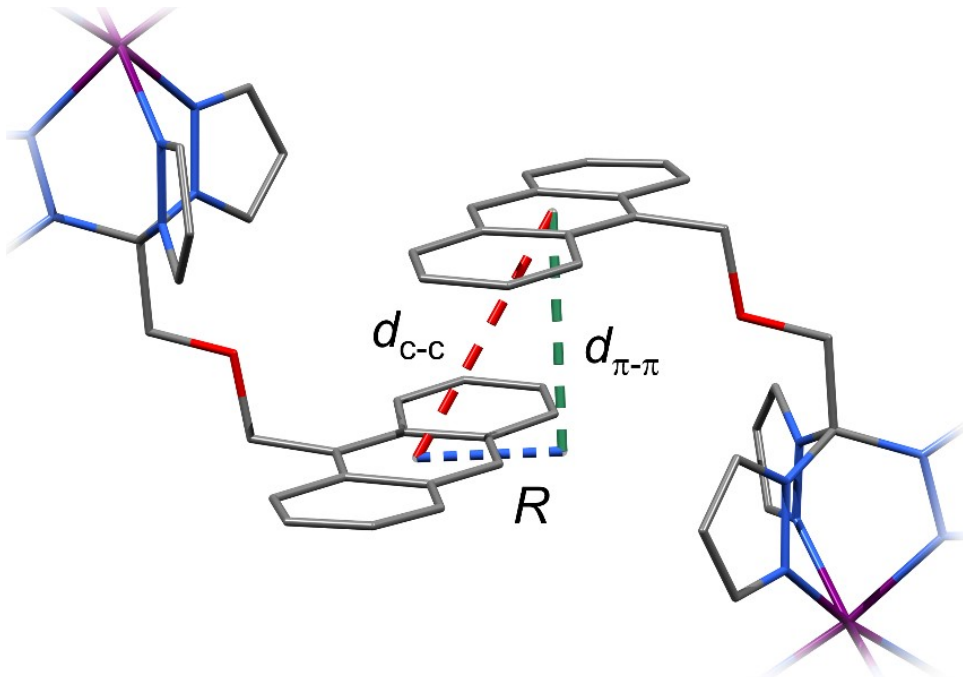

Figure S20. Anthracene dimmer in crystal of **1** and **2**.

Table S1. Single Crystal diffraction data of **1** and **2**.

Identification code	**1**	**2**
Empirical formula	$C_{212}H_{230}B_4Co_4F_{12}Fe_4N_{76}O_{23}S_4$	$C_{213}H_{221}B_4Co_4F_{21}Fe_4N_{76}O_{27}S_7$
Formula weight	5069.31	5403.42
Temperature/K	99.91	109.89
Crystal system	triclinic	triclinic
Space group	$P\bar{1}$	$P\bar{1}$
a/Å	19.4205(9)	18.6217(8)
b/Å	20.0866(11)	20.0661(7)
c/Å	34.3463(17)	36.4748(14)
α/°	93.235(2)	96.0810(10)
β/°	92.907(2)	91.5700(10)
γ/°	108.862(2)	100.7960(10)
Volume/Å^3	12624.8(11)	13297.2(9)
Z	2	2
ρ_{calc}g/cm^3	1.334	1.350
μ/mm^{-1}	0.596	0.598
F(000)	5244.0	5560.0
Crystal size/mm^3	0.5 × 0.3 × 0.2	0.55 × 0.38 × 0.31
Radiation	MoKα (λ = 0.71073)	MoKα (λ = 0.71073)
2Θ range for data collection/°	4.444 to 49.636	4.446 to 49.606

Index ranges	-22 ≤ h ≤ 22, -23 ≤ k ≤ 23, -40 ≤ l ≤ 40	-21 ≤ h ≤ 21, -23 ≤ k ≤ 23, -42 ≤ l ≤ 43
Reflections collected	120789	153765
Independent reflections	43028 [R_{int} = 0.0597, R_{sigma} = 0.0761]	45483 [R_{int} = 0.0873, R_{sigma} = 0.0962]
Data/restraints/parameters	43028/1400/3037	45483/2393/3916
Goodness-of-fit on F^2	1.033	1.025
Final R indexes [I>=2σ (I)]	R_1 = 0.0944, wR_2 = 0. 0.2522	R_1 = 0.0907, wR_2 = 0.2513
Final R indexes [all data]	R_1 = 0.1501, wR_2 = 0.3098	R_1 = 0.1255, wR_2 = 0.2950
Largest diff. peak/hole / e Å^{-3}	1.54/-0.86	1.17/-0.97

Table S2. The selected bond length of complex **1**.

Co1		**Co2**	
Co1–N7	2.076(5)	Co2–N10	2.061(5)
Co1–N8	2.081(6)	Co2–N11	2.060(6)
Co1–N9	2.078(6)	Co2–N12	2.064(6)
Co1–N19	2.109(5)	Co2–N22	2.104(5)
Co1–N20	2.106(5)	Co2–N23	2.132(5)
Co1–N21	2.112(5)	Co2–N24	2.112(5)
Co3		**Co4**	
Co3–N1	2.071(5)	Co4–N4	2.061(5)
Co3–N2	2.072(5)	Co4–N5	2.074(5)
Co3–N3	2.059(5)	Co4–N6	2.049(6)
Co3–N13	2.115(5)	Co4–N16	2.118(5)
Co3–N14	2.121(5)	Co4–N17	2.117(5)
Co3–N15	2.144(6)	Co4–N18	2.125(5)
Fe1		**Fe2**	
Fe1–C7	1.956(7)	Fe2–C10	1.969(8)
Fe1–C8	1.934(7)	Fe2–C11	1.936(7)
Fe1–C9	1.928(7)	Fe2–C12	1.962(7)
Fe1–N31	1.989(5)	Fe2–N34	1.973(6)
Fe1–N32	1.976(5)	Fe2–N35	1.949(5)
Fe1–N33	1.977(6)	Fe2–N36	1.983(6)
Fe3		**Fe4**	
Fe3–C1	1.944(6)	Fe4–C4	1.949(6)
Fe3–C2	1.934(6)	Fe4–C5	1.938(7)
Fe3–C3	1.943(6)	Fe4–C6	1.950(7)
Fe3–N25	1.975(5)	Fe4–N28	2.000(5)
Fe3–N26	1.969(4)	Fe4–N29	1.987(5)
Fe3–N27	1.978(5)	Fe4–N30	1.989(5)

Table S3. Selected bond length of complex **2**.

Co1		**Co2**	
Co1–N1	2.091(4)	Co2–N4	2.070(4)
Co1–N2	2.081(4)	Co2–N5	2.057(4)
Co1–N3	2.068(4)	Co2–N6	2.080(4)
Co1–N13	2.133(4)	Co2–N19	2.150(4)
Co1–N14	2.095(4)	Co2–N20	2.105(4)
Co1–N15	2.165(4)	Co2–N21	2.111(4)
Co3		**Co4**	
Co3–N7	2.073(5)	Co4–N10	2.077(4)
Co3–N8	2.078(4)	Co4–N11	2.078(5)
Co3–N9	2.070(5)	Co4–N12	2.076(5)
Co3–N34	2.126(6)	Co4–N25	2.128(4)
Co3–N35	2.110(6)	Co4–N26	2.116(4)
Co3–N36	2.124(5)	Co4–N27	2.133(4)
Fe1		**Fe2**	
Fe1–C1	1.926(5)	Fe2–C4	1.910(5)
Fe1–C2	1.923(5)	Fe2–C5	1.924(5)
Fe1–C3	1.942(6)	Fe2–C6	1.924(5)
Fe1–N16	1.993(4)	Fe2–N22	1.971(4)
Fe1–N17	1.958(4)	Fe2–N23	1.961(4)
Fe1–N18	1.960(4)	Fe2–N24	1.964(4)
Fe3		**Fe4**	
Fe3–C7	1.928(6)	Fe4–C10	1.936(5)
Fe3–C8	1.919(5)	Fe4–C11	1.915(6)
Fe3–C9	1.920(6)	Fe4–C12	1.939(6)
Fe3–N31	1.970(5)	Fe4–N28	1.973(5)
Fe3–N32	1.971(4)	Fe4–N29	1.961(5)
Fe3–N33	1.965(5)	Fe4–N30	1.966(5)

Table S4. Average Co–N bond length and continuous shape measurement of Co centers.

	1	**2**
Average Co–$N_{cyanide}$ bond length (Å)	2.067	2.075
Average Co–N_{ligand} bond length (Å)	2.118	2.125
CShMCo	0.217	0.271